PHILOSOPHICAL TRANSACTIONS OF THE ROYAL SOCIETY A MATHEMATICAL, PHYSICAL & ENGINEERING SCIENCES

Damage Tolerant Fibre Reinforced Sheet Metal Composites

I. R. McColl and J. G. Morley

Phil. Trans. R. Soc. Lond. A 1977 **287**, 17-43
doi: 10.1098/rsta.1977.0138

DAMAGE TOLERANT FIBRE REINFORCED SHEET METAL COMPOSITES

By I. R. McColl and J. G. Morley
Wolfson Institute of Interfacial Technology, University of Nottingham, England

(*Communicated by Sir Alan Cottrell, F.R.S. – Received 22 October* 1976)

CONTENTS

Theoretical and experimental studies have been made of the effect of non-fracturing reinforcing members on the growth of a central crack in metal and polymeric sheets subjected to a uniform tensile load. The crack has been aligned perpendicularly to the reinforcing members which have been oriented in the same direction as the applied load.

As a consequence of interactions between the non-fracturable and fracturable components of the composite structure, crack growth in the latter is inhibited severely. At the same time the non-fracturing reinforcing members provide a residual fail-safe load bearing capability.

Tolerable agreement is observed between the predictions of the proposed theory and the observed behaviour of experimental samples.

Vol. 287. A 1388. 3 [Published 18 August 1977

1. Introduction

Research on fibre reinforced metals was initiated in the early 1960s because of the potential engineering advantages to be gained by replacing a polymeric matrix with a metal. It was expected that the development of metal matrix composites would enable the temperature limitations of polymers to be avoided while, at the same time, the need for multi-directional arrays of reinforcing fibres would be reduced because of the superior mechanical properties of metals. It was thought that metal matrix systems were more likely to be compatible with existing metal structures and to be more resistant to surface damage than polymers. Furthermore, it was hoped that the superior toughness of metals would be reflected in the properties of the composites.

From the outset emphasis was given to the use of ceramic reinforcing fibres because of the combination of high specific strength, high specific stiffness and high temperature capability which these materials possess. A number of ceramic fibre-reinforced composite systems have been produced on a laboratory scale but only one system, boron/aluminium, has been manufactured in engineering quantities. Chemical and physical interactions between fibre and matrix, encountered during fabrication, have been largely responsible for the very limited range of fibre-reinforced metals produced. These problems have been reduced to manageable proportions by the use of two-stage fabrication procedures which utilize hot pressing techniques as a final step. The properties of ceramic fibre reinforced metals have been reviewed recently by Morley (1976).

The fabrication of boron/aluminium composites is facilitated by the low melting temperature of aluminium but, even so, it is impracticable to hot press large structures in one operation because of the very large presses which would be required. As a consequence incremental multiple step pressing procedures have been investigated (Prewo 1976). Compatibility problems can be avoided by the use of controlled solidification to produce the reinforcing component by phase separation, but this technique is only applicable to small engineering components.

In order to widen the choice of materials used and to maximize the contribution of relatively expensive ceramic fibres, the principle of selective reinforcement has been developed (Zender & Dexter 1968; Mayer 1974). This technique is based on hybrid structures consisting of a metal substrate to which polymer-bonded ceramic fibres are attached. A metal beam having ceramic fibres bonded to its upper and lower surfaces, so that they are most effective during flexure, is a simple example of this approach. The selective reinforcement of a metal substrate offers a further advantage, in that it can be arranged for the metallic portion of the material to carry the design loads applied to the structure while the ceramic fibres contribute additional stiffness. In this way, the relatively unpredictable fracture behaviour of fibrous composites (Hancock 1974) can be more easily accommodated in an engineering design philosophy. However, with this approach, the metal component of the structure is still susceptible to fatigue failure.

When the loads are applied in the direction of the fibre alignment the fatigue characteristics of metals, in which reinforcing ceramic fibres are embedded, are much superior to those of unreinforced metals. The failure process is general and progressive instead of being localized and catastrophic, as is usually the case with unreinforced metals. The ability of fibres to deflect fatigue cracks in the matrix and to carry loads across the fracture faces is similar to the engineering use, on a larger scale, of local reinforcement by 'crack stoppers' to limit the growth of fatigue cracks in sheet metal structures. The reinforcing fibres do not, of course, provide these benefits when cyclic loads are applied transversely to the direction of fibre alignment.

When a monotonically increasing tensile load is applied along the direction of fibre alignment,

fibre-reinforced metals fracture in a localized region at a low overall strain value in the region of 1 %. The strain-hardening characteristics of the matrix cannot stabilize the failure process because of the small volume of metal which undergoes plastic deformation. Similar low failing strains and localized failure are also experienced under traverse tensile loading. Under both these loading conditions, therefore, existing fibre reinforced metals can be considered to behave as brittle materials.

In an attempt to avoid the engineering limitations of existing metal matrix fibrous composites which have been outlined above, preliminary investigations have been carried out on an alternative approach to the design of reinforced sheet metal systems. These systems differ from existing fibre-reinforced metals in the following ways.

(1) Fabrication can be carried out by using conventional sheet metal shaping and joining techniques. Hence, in principle, a wide variety of materials can be utilized in the construction of the composite systems. As a consequence of the fabrication procedures followed, the systems would be expected to be quite compatible with existing sheet metal structural components.

(2) The primary reinforcing members do not fracture and thus provide a residual fail-safe characteristic. In addition they provide two alternative mechanisms by which crack growth in the metal sheet is inhibited. In the first case, which is treated in this paper, crack growth is inhibited through a reduction in the amount of strain energy released in the presence of a crack and also through additional frictional energy losses occurring during crack growth. These effectively enhance the work of fracture of the metal sheet. In the second case, which will be discussed elsewhere, the primary reinforcing members are prestressed in tension with the rest of the composite structure in residual compression. This approach seems likely to be of particular value in suppressing the initiation and growth of fatigue cracks in a metal sheet.

(3) It seems feasible to incorporate two separate sets of reinforcing members in a composite sheet metal structure of this type. One set (the non-fracturing members) would provide damage tolerance and a residual tensile load bearing capability as described above. The other would provide increased specific stiffness values. This reinforcing component could be formed from ceramic fibres bonded to the sheet metal in a similar manner to the selective reinforcement principle mentioned previously. These possibilities are discussed in the conclusions of this paper.

The basic principle of the non-fracturing behaviour of the primary reinforcing members used in this study has been described by Morley (1970). The non-fracturing characteristic is achieved through the use of a stress-controlled decoupling/recoupling mechanism acting at the interface between the reinforcing members and the rest of the composite structure. The strength in shear of this interface is arranged to decrease as the tensile load carried by the reinforcing member increases. This contrasts with the behaviour of conventional composites where the shear stress transfer rate has, in effect, a constant value.

The maximum tensile load carried by the primary reinforcing members, as a result of tensile deformation occurring in the rest of the composite structure, is limited to that at which complete debonding of the interface occurs. This is arranged to be less than the tensile breaking load of the reinforcing members so that they cannot fracture under overload conditions. Thus, they are insensitive to stress concentrations occurring in the matrix and remain intact carrying a load across a matrix crack, whatever the magnitude of the separation of the crack faces. The composite system has a fail-safe characteristic in that the load bearing ability of the primary reinforcing members is always retained.

PHILOSOPHICAL TRANSACTIONS OF THE ROYAL SOCIETY A MATHEMATICAL, PHYSICAL & ENGINEERING SCIENCES

The design of reinforcing elements having these characteristics has been described by Morley & Millman (1974) and by Chappell, Morley & Martin (1975). They consist of two elastic components, a core and a tubular sheath. The core, which is the primary reinforcing member, is circular in section and convoluted, usually helically, with a helix angle in the region of 85°. The helix has a larger overall diameter than the internal diameter of the sheath so that, when in place within the sheath, it exerts a strong pressure on the walls of the sheath. Hence a strong frictional force is generated which resists the displacement of the core. Stainless steel hypodermic tubes with steel wire cores have been used in the construction of the core/sheath (duplex) systems studied so far. The contact pressure and frictional force are reduced progressively and reversibly as the tensile load carried by the helix is increased. Complete debonding occurs when the overall diameter of the helix is reduced to that of the internal diameter of the tube.

It is observed experimentally (Morley & Millman 1974) that the load L required to withdraw or insert a length x of the core member is given by an equation of the form

$$L = L_{\max}(1 - e^{-kx}), \tag{1}$$

where $L_{\max}$ is the limiting debonding load and k is a constant. More recent studies (Morley, Millman & Martin 1976) show that the limiting stress distribution along a core member as it is being withdrawn from its tube follows the same relationship. As a result of the large hoop tensile stresses which are developed in the tube and the large effective Poisson ratio of the helical core, its longitudinal stiffness is enhanced considerably when constrained by the tube. This effect, coupled with the fact that the core member is in any event almost straight, ensures that the longitudinal stiffness of the convoluted core, when inside the tube, is comparable with the Young modulus of a straight member formed from the same material and having the same cross-sectional area.

The core reinforcing members also differ from conventional reinforcing fibres in that it can be arranged for the core member to be prestressed in tension with the tube member, and any matrix to which it is attached, in residual compression. As mentioned previously, this feature is clearly of particular importance in the suppression of the initiation and growth of fatigue cracks in a reinforced metal sheet. Preliminary studies of the behaviour of steel wire core/stainless steel sheath systems have been reported by McColl & Morley (1975). More recent studies have shown that fatigue lifetimes in excess of 10^6 cycles at core peak stress values of about 1 GPa can be obtained with similar steel core steel tube elements (McColl & Morley 1977*a*).

The work reported in this paper has been carried out on experimental systems consisting of a sheet of metal or polymer to the surface of which has been attached a layer of bicomponent reinforcing elements of the type described above. A uniform tensile load has been applied to the edges of the specimens in the same direction as that of the fibre alignment. The width of the specimens tested has ranged from 0.12 m to 0.915 m and they have contained initial central cracks having lengths ranging from *ca.* 0.04 m to 0.2 m. The initial crack lengths have been arranged perpendicularly to the direction of fibre alignment.

The analytical work reported here has been concerned with systems in which all the components are initially under zero longitudinal differential stress and the sheet has been considered to be semi-infinite in extent and to be subjected to uniform tensile loads applied at its remote edges. Computed strain distributions around cracks of various lengths in a reinforced aluminium sheet are reported. A 30% volume fraction of duplex reinforcing elements (core plus tube) is considered, in which the cross-sectional areas of core and tube are equal. The tubes are considered

to behave as part of the matrix. Calculations have been made of the rate of release and the rate of absorption of energy for this system for increasing crack lengths and for elastic strain values extending up to 0.004. Similar calculations have been carried out to account for the behaviour of the various experimental specimens studied and these are compared with the experimental results obtained.

It is possible that sheet metal systems reinforced with steel duplex elements of the type described in this paper can be used with little modification in certain types of advanced engineering applications. Hypodermic tubes are intrinsically relatively inexpensive in comparison with boron fibres. However, other composite configurations, possessing similar mechanical characteristics but with the tube and matrix assembly manufactured from sheet metal, can be envisaged (Morley 1976; Morley *et al.* 1976). These may offer advantages from the point of view of manufacturing convenience.

The studies reported here refer to unidirectionally reinforced sheet materials subjected to a uniform tensile stress. Consideration also needs to be given to non-uniform and unconventional loading conditions. One situation of particular interest concerns the applications of concentrated loads to an engineering structure directly through the core reinforcing members. This approach would seem to be perfectly feasible where the primary reinforcing members are formed from strong metal wires and may offer a convenient means of applying a concentrated load to a highly stressed sheet metal structure.

Since the stress transfer mechanism between the core and the sheath in these systems in due to frictional effects, it is of interest to establish the effects of conventional lubricants on this frictional interaction. Preliminary studies indicate that the presence of conventional lubricants has no noticeable effect on the frictional stress transfer between core and sheath (Morley & Chappell 1977). It appears, therefore, that the presence of lubricants would not be deleterious in the case of metal reinforcing members and might be used to advantage in certain corrosive environments.

2. Critical energy rate analysis of crack behaviour

2.1. *Crack stability under uniform loading conditions*

The prediction, based on energetic principles, of the behaviour of a crack in a composite structure acting under applied loads is concerned with the rates of release and of absorption of strain energy associated with crack growth. The condition necessary for such a crack to be able to grow without work being done by the applied loads, i.e. the condition necessary for catastrophic crack growth, is the Griffith criterion, namely,

$$\mathrm{d}W_{\mathrm{R}}/\mathrm{d}(2a) \geqslant \mathrm{d}W_{\mathrm{A}}/\mathrm{d}(2a),$$

where $\mathrm{d}W_{\mathrm{R}}/\mathrm{d}(2a)$ is the rate of release of strain energy for a crack of length $2a$ under fixed grip loading conditions, $\mathrm{d}W_{\mathrm{A}}/\mathrm{d}(2a)$ is the rate of absorption of energy at the onset of crack growth, due to the work of fracture of the fracturable part of the structure and any other effects such as relative displacements between components of the structure against resisting frictional forces. For conventional elastic materials the necessary energetic condition for catastrophic crack growth is given by the well-known Griffith equation,

$$\sigma = (EGm/\pi a)^{\frac{1}{2}},$$

where σ is the fracture stress of the material, E is the Young modulus, Gm is the work of fracture value pertaining to the initiation of fracture and $2a$ is the crack length.

When a non-fracturable reinforcing component is present it interacts with the fracturable part of the composite structure modifying the strain field around the crack and hence the rate of release of strain energy. Also this interaction results in the non-recoverable absorption of strain energy by work done against frictional forces and thus contributes to the rate of absorption of strain energy.

2.2. *Theoretical strain distribution*

This analysis is concerned with the behaviour of a central crack in a thin sheet structure uniaxially and uniformly reinforced with non-fracturing reinforcing elements. Uniform uniaxial loading perpendicular to the plane of the crack and parallel to the direction of reinforcement is considered. The crack lengths are assumed small, compared with the size of the sheet, but sufficiently long for any plastic zone around the crack tips to be fully developed.

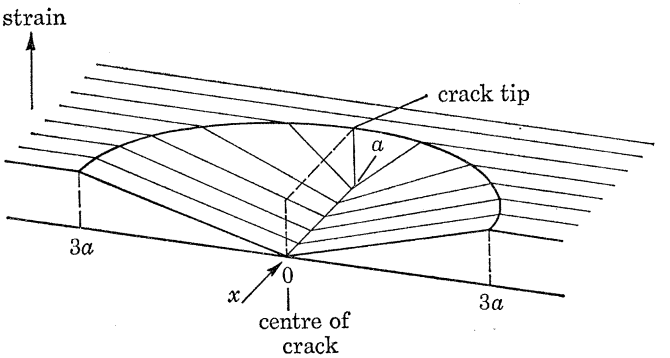

FIGURE 1. Idealized strain field around a crack in an unreinforced sheet.

Prediction of the behaviour of a crack requires the rates of release and of absorption of strain energy, as a function of crack length, to be calculated. To do this a knowledge of how the strain energy is released and redistributed during crack growth is necessary. Also the degree of relative displacement between the core and sheath of the reinforcing elements, during crack growth, is required to enable the work done against frictional forces to be calculated. Thus, a representation of the strain field around the crack is first obtained. The form of the strain field and the general physical model considered has been discussed previously by Morley & McColl (1975) and only a brief outline will be given here.

The model assumes an elliptical zone around the crack to be partially relaxed. For the unreinforced sheet a linear change in strain is assumed, parallel to the direction of loading, from the crack face to the extremities of the elliptical zone (figure 1). The size of the elliptical zone is chosen such that the strain energy released by the presence of the crack, on the basis of the assumptions made, is the same as calculated by Griffith (1920) for the classical case of a crack in an infinite elastic material. It follows that the major axis of the ellipse is three times the crack length. Outside the partially relaxed elliptical zone the sheet is assumed to be unaffected by the presence of the crack. Only strains parallel to the direction of loading are considered and shear interactions between the adjacent strips, together with stress concentration at the crack tips, are neglected. The validity of these assumptions is discussed in § 3.

2.3. *Theoretical equations describing the strain field around a crack bridged by non-fracturing reinforcing elements*

In order to simplify computation of the effects of the duplex (non-fracturing) reinforcing elements, the exponential form of the stress distribution along an element is reduced to that of a constant shear strength interface up to a stress level σ_d, and corresponding strain ϵ_d, at which complete debonding is assumed to occur (figure 2).

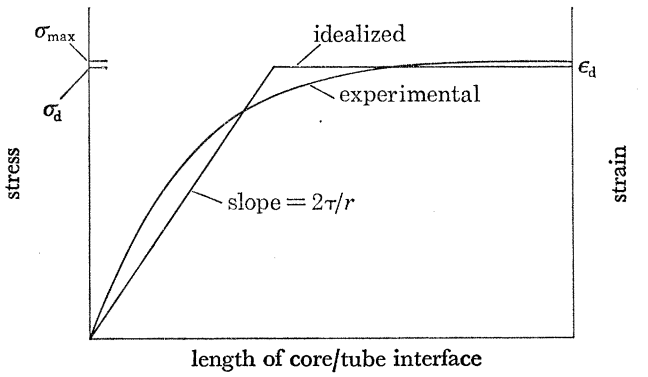

FIGURE 2. Idealized and experimental strain distributions along the core element of a non-fracturing reinforcing element.

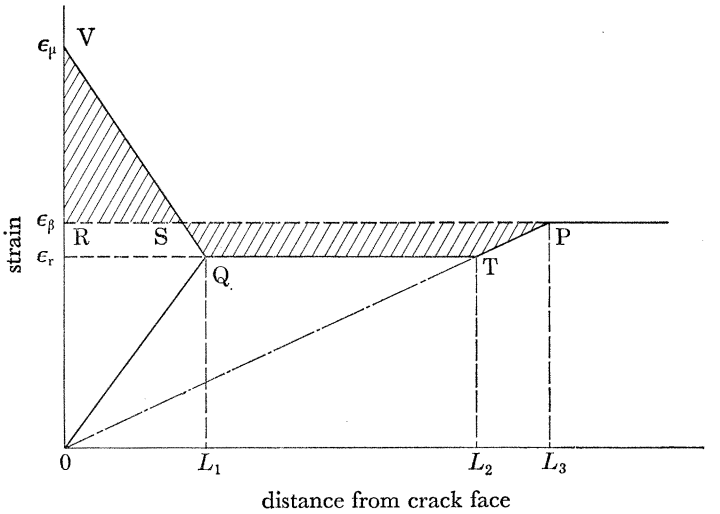

FIGURE 3. Strain distribution along a section perpendicular to a crack in a sheet reinforced with non-fracturing reinforcing elements ($\epsilon_\mu < \epsilon_d$).

The longitudinal strain distribution along a section perpendicular to the plane of a crack in a duplex reinforced sheet is shown in figure 3. The maximum core element strain ϵ_μ is taken to be less than the debonding strain ϵ_d. The core elements bridge the crack and load is transferred from the core elements to the tube/sheet assembly in the vicinity of the crack (from O to L_1). For the purpose of this analysis the tube (sheath) elements are assumed to behave as part of the sheet (matrix) although their contributions to the work of fracture and stiffness of the structure are

taken into account. The rates of change of core element strain and matrix strain in the region of the crack (i.e. the slopes of the lines VQ and OQ in figure 3) are given by,

$$\frac{\mathrm{d}\epsilon_{\mathrm{f}}}{\mathrm{d}x} = -\frac{2\tau}{E_{\mathrm{f}} r} \tag{2}$$

and

$$\frac{\mathrm{d}\epsilon_{\mathrm{m}}}{\mathrm{d}x} = \frac{2V_{\mathrm{f}}\tau}{(E_{\mathrm{m}}V_{\mathrm{m}} + E_{\mathrm{t}}V_{\mathrm{t}})\, r} + \frac{\epsilon_\beta}{L_3} \tag{3}$$

respectively, where

r is taken as the radius of the wire from which the core element is formed.

τ is the effective shear strength of the core/tube element interface measured over the surface area of the core wire.

E_{f}, E_{t} and E_{m} are the Young moduli of the core elements, tube elements and sheet respectively.

V_{f}, V_{t} and V_{m} are the volume fractions of the core elements, tube elements and sheet respectively.

ϵ_β/L_3 is the strain gradient along the section in the absence of the reinforcing elements.

ϵ_β is the general strain in the structure outside the elliptical zone.

L_3 is the distance from the plane of the crack to the edge of the elliptical zone and is given by,

$$L_3 = 3(a^2 - x^2)^{\frac{1}{2}},$$

where a is the half crack length and x is the distance from the centre of the crack to the section considered.

At the position L_1 (figure 3) the elastic strains of the core elements and the tube/sheet assembly are the same and thus the differential movement between the components is zero. Hence, no further stress transfer between the core elements and the tube/sheet assembly occurs and it is assumed that from position L_1 to position L_2 the elastic strain in both core elements and tube/sheet assembly remains the same. From position L_2, which lies on the strain distribution for the unreinforced sheet, to position L_3, which is on the edge of the ellipse, the strain distributions for both the core elements and the tube/sheet assembly are assumed to be the same and to correspond with those of the sheet with the core elements absent. Since the strain redistributions, due to the presence of the crack, are assumed to occur entirely within the partially relaxed elliptical zone, the total integrated strain of the core elements must be unchanged by the presence of the crack. Thus, in figure 3, the areas shown shaded must be equal. This boundary condition together with equations (2) and (3) enables equations defining the strain distribution along any section in the elliptical zone, perpendicular to the plane of the crack, to be derived. These are,

$$\left.\begin{aligned} \epsilon_{\mathrm{r}} &= [\epsilon_\beta L_3/\{Q(P + \epsilon_\beta/L_3)^{-2} + L_3/\epsilon_\beta\}]^{\frac{1}{2}}, \\ \epsilon_\mu &= L_1(P + Q + \epsilon_\beta/L_3), \\ L_1 &= \epsilon_{\mathrm{r}}(P + \epsilon_\beta/L_3)^{-1},\ L_2 = L_3\epsilon_{\mathrm{r}}/\epsilon_\beta,\ L_3 = 3(a^2 - x^2)^{\frac{1}{2}}, \end{aligned}\right\} \tag{4}$$

where $P = 2V_{\mathrm{f}}\tau/(E_{\mathrm{m}}V_{\mathrm{m}} + E_{\mathrm{t}}V_{\mathrm{t}})\, r$ and $Q = 2\tau/E_{\mathrm{f}} r$,

ϵ_{r}, ϵ_μ, ϵ_β, L_1, L_2, L_3 are defined in figure 3.

The half crack opening, at a distance x from the centre of the crack, is obtained from the difference in integrated strain between the core elements and the tube/sheet assembly, over the distance OL_1, and is given by $\mu = \frac{1}{2}\epsilon_\mu L_1$.

So far, it has been assumed that the stress supported by the reinforced structure is such that the crack-bridging core reinforcing elements, in the section considered, are not stressed to their

debonding level. If the core elements do reach their debonding stress, in the vicinity of the crack, the model assumes that they suddenly decouple from the tube/sheet assembly.

Figure 4 shows the strain distribution along a section, perpendicular to the plane of the crack, appropriate to such a situation. From the face of the crack to the point L_0 the core elements are completely decoupled from the tube/sheet assembly. Between L_0 and L_1 load is transferred between the core elements and the tube/sheet assembly via the assumed constant shear strength interface. From L_1 to the edge of the ellipse the strain distribution is as defined for the non-decoupled core elements shown in figure 3. Again the integrated strain of the core elements is unchanged by the presence of the crack so that the areas shown shaded in figure 4 are equal.

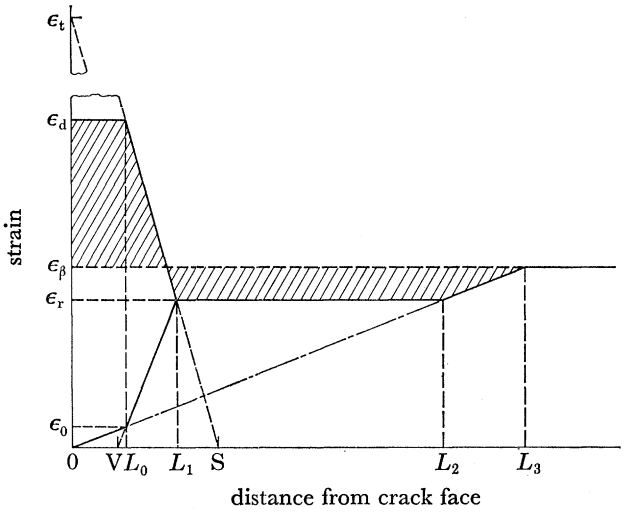

FIGURE 4. Strain distribution along a section perpendicular to a crack in a sheet reinforced with non-fracturing reinforcing elements ($\epsilon_\mu = \epsilon_d$).

Thus, as for the case of the non-decoupled core elements, a set of equations describing the strain distribution along any section in the elliptical zone perpendicular to the plane of the crack may be derived. These are

$$\left.\begin{aligned} \epsilon_r &= [C\epsilon_d - \{2C(\epsilon_d^2 - \epsilon_\beta^2)\}^{\frac{1}{2}}]/C, \\ \epsilon_0 &= L_0\epsilon_\beta/L_3, \\ L_0 &= L_3[\epsilon_r - (P + \epsilon_\beta/L_3)\,(\epsilon_d - \epsilon_r)/Q]/\epsilon_\beta, \\ L_1 &= L_3[\epsilon_r - P(\epsilon_d - \epsilon_r)/Q]/\epsilon_\beta, \\ L_2 &= \epsilon_r L_3/\epsilon_\beta, \\ L_3 &= 3(a^2 - x^2)^{\frac{1}{2}}, \end{aligned}\right\} \tag{5}$$

where

$$C = 2\{1 + (2P + \epsilon_\beta/L_3)/Q\},$$

$$P = 2V_f\tau/(E_mV_m + E_tV_t)\,r,$$

$$Q = 2\tau/E_f r.$$

ϵ_r, ϵ_d, ϵ_0, L_0, L_1, L_2, L_3 are defined as in figures 3 and 4.

The half crack opening μ is now given by,

$$\mu = \epsilon_d(L_0 + L_1)/2 - L_0L_1\epsilon_\beta/2L_3.$$

PHILOSOPHICAL TRANSACTIONS OF THE ROYAL SOCIETY A MATHEMATICAL, PHYSICAL & ENGINEERING SCIENCES

The sets of equations (4) and (5) enable the complete theoretical strain field around a crack in a duplex reinforced sheet to be described in terms of the mechanical parameters of the structure, the general strain outside the partially relaxed elliptical zone and the crack length. The strain field for one quadrant of the partially relaxed ellipse is obtained by first computing the strain distribution along a section near the crack tip and then along similar sections nearer to the centre

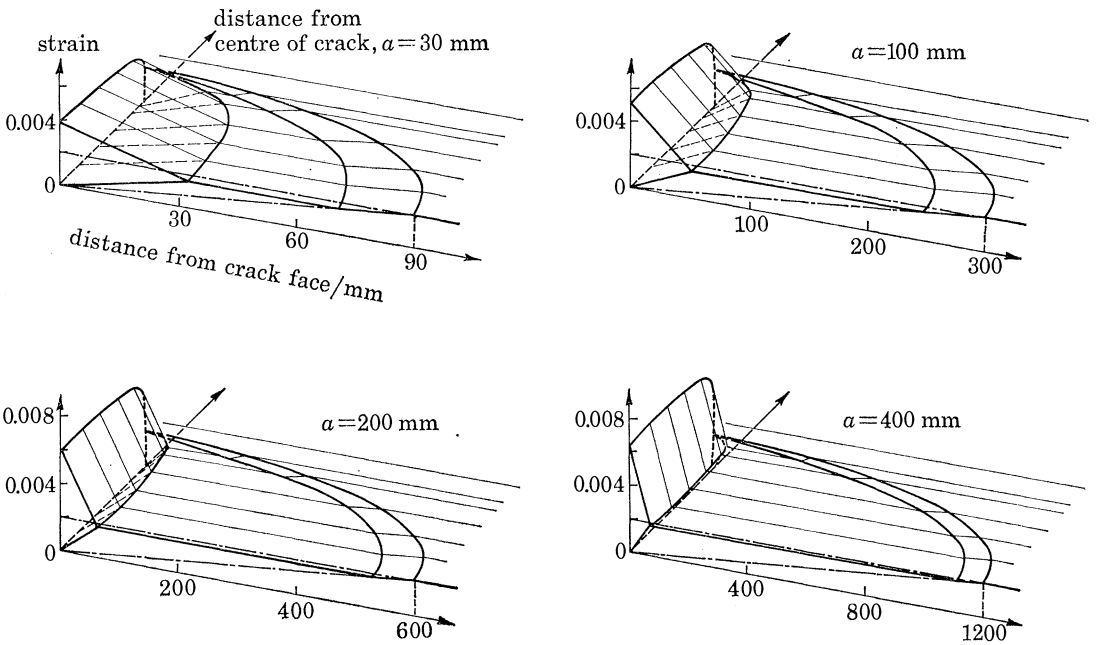

FIGURE 5. Computed strain field development around a crack of increasing length ($2a$) in a sheet reinforced with non-fracturing reinforcing elements ($\epsilon_c > \epsilon_\beta = 0.002$).

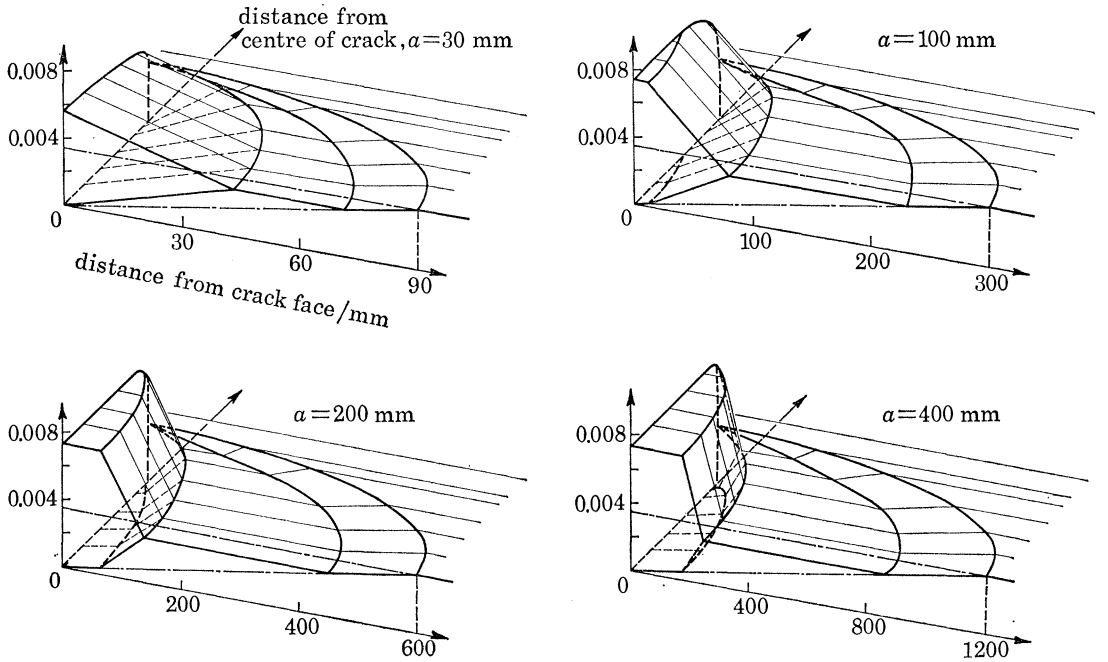

FIGURE 6. Computed strain field development around a crack of increasing length ($2a$) in a sheet reinforced with non-fracturing reinforcing elements ($\epsilon_c < \epsilon_\beta = 0.0035$).

of the crack using equations (4). The position of these sections is controlled by the value of x, the distance along the crack face from the centre of the crack. The value of ϵ_μ at each section is inspected and where it exceeds ϵ_d the strain distribution is recalculated using equations (5). The strain fields for the other quadrants of the ellipse are obtained from symmetry.

2.4. *Numerical values of strain fields around a crack*

Figures 5 and 6 show examples of strain fields around cracks in a duplex reinforced sheet computed using equations (2), (3), (4) and (5) from the parameters given in table 1. Figure 5 shows the development of the strain field, for increasing crack lengths, for the value of bulk strain ($\epsilon_\beta = \epsilon_c$) at which the core elements are just capable of supporting the whole applied load. Figure 5 shows that, irrespective of crack length, the core elements nowhere reach their debonding strain levels provided $\epsilon_\beta \leqslant \epsilon_c$. Figure 6 shows the strain field development, for increasing crack length, for a value of bulk strain ($\epsilon_\beta > \epsilon_c$) under which condition the core elements are not capable of supporting the whole applied load. It is apparent that both the fraction of debonded core elements bridging the crack and the debonded length of the core elements increases with increasing crack length.

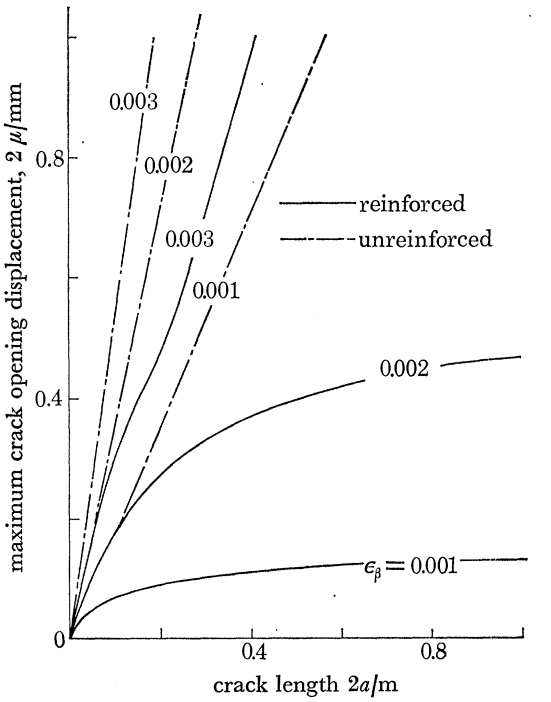

FIGURE 7. Maximum crack opening displacement as a function of crack length and applied strain for both an unreinforced sheet and a sheet reinforced with non-fracturing reinforcing elements.

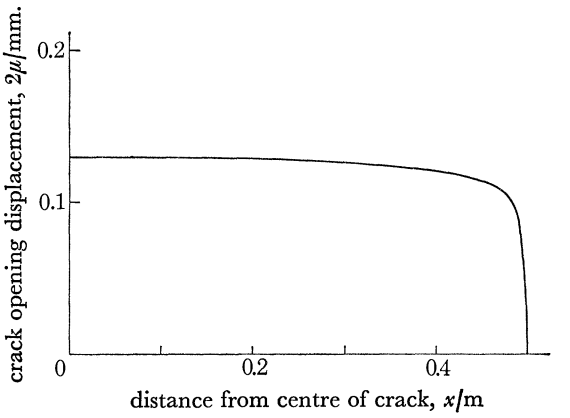

FIGURE 8. Profile of a crack in a sheet reinforced with non-fracturing reinforcing elements ($\epsilon_\beta < \epsilon_c$).

Values of maximum crack opening displacement (at the centre of the crack, computed from the data given in table 1) as a function of crack length for both unreinforced and duplex reinforced sheets, are shown in figure 7. It will be observed that for $\epsilon_\beta \leqslant \epsilon_c$ the maximum crack opening displacement tends to a limiting value with increasing crack length. For $\epsilon_\beta > \epsilon_c$ the maximum crack opening displacement is dependent on crack length but is reduced compared with the

unreinforced case. Figure 8 shows a crack profile computed using the parameters in table 1. It shows that, for $\epsilon_\beta \leqslant \epsilon_c$ and for cracks of sufficient length, the profile of a crack in a sheet reinforced with non-fracturing reinforcing elements tends to that of a parallel-sided crack under conditions of uniaxial uniform loading.

2.5. *Theoretical equations of strain energy release*

The strain energy released by a section of sheet reinforced with non-fracturing reinforcing elements, having a width δx and of unit thickness, may be computed from the strain distribution along the section. If the core elements in the section are not loaded to their debonding level, the energy released (δW_{Rx}) by a section at a distance x from the centre of the crack is given by Morley & McColl (1975) as

$$\delta W_{Rx} = [\tfrac{1}{2}E_c\epsilon_\beta^2 L_3 - \tfrac{1}{6}E_c\epsilon_\beta^2(L_3^3 - L_2^3)/L_3^2 - \tfrac{1}{2}E_c\epsilon_r^2(L_2 - L_1) - \tfrac{1}{6}E_{mt}\epsilon_r^2 L_1 - \tfrac{1}{6}V_f E_f(\epsilon_\mu^2 + \epsilon_\mu\epsilon_r + \epsilon_r^2)\, L_1]\,\delta x, \quad (6)$$

where $L_3 = 3(a^2 - x^2)^{\frac{1}{2}}$; $E_c = E_f V_f + E_m V_m + E_t V_t$; and $E_{mt} = E_m V_m + E_t V_t$.

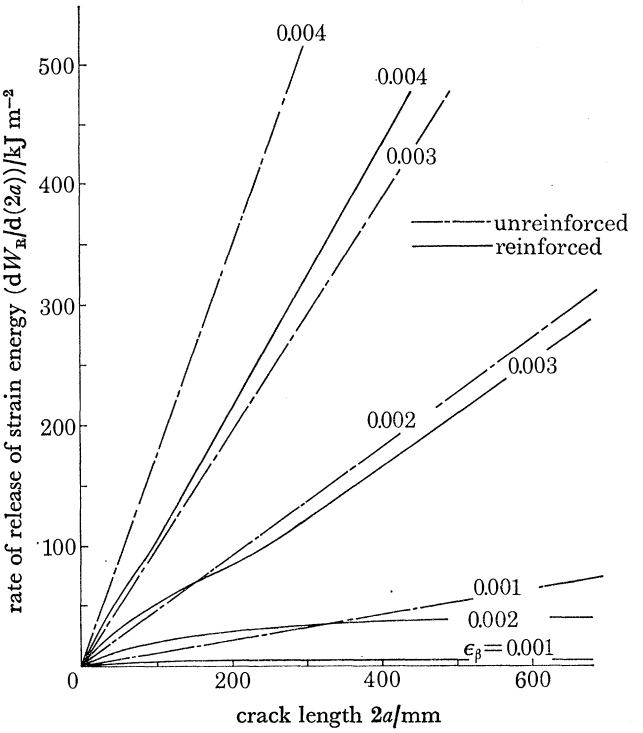

FIGURE 9. Rates of release of strain energy for an unreinforced sheet and a sheet reinforced with non-fracturing reinforcing elements, computed using the values listed in table 1.

If the core elements in the section are loaded to their debonding level, the energy released is given by

$$\delta W_{Rx} = \Big[\tfrac{1}{2}E_c\epsilon_\beta^2 L_3 - \tfrac{1}{6}E_c\epsilon_\beta^2(L_3^3 - L_2^3)/L_3^2 - \tfrac{1}{2}E_c\epsilon_r^2(L_2 - L_1) - \tfrac{1}{6}E_{mt}\epsilon_\beta^2 L_0^3/L_3^2 - \tfrac{1}{2}E_{mt}\left(\frac{\epsilon_r - \epsilon_0}{L_1 - L_0}\right)^2 \times \{\tfrac{1}{3}L_1^3 - \tfrac{1}{3}L_0^3 - V(L_1^2 - L_0^2) + V^2(L_1 - L_0)\} - \tfrac{1}{2}V_f E_f \epsilon_d^2 L_0 - \tfrac{1}{6}(V_f E_f/S^2)\,\epsilon_t^2\{(S - L_0)^3 - (S - L_1)^3\}\Big]\,\delta x, \quad (7)$$

where

$$V = \frac{\epsilon_r L_0 - \epsilon_0 L_1}{\epsilon_r - \epsilon_0}; \quad S = \frac{\epsilon_d L_1 - \epsilon_r L_0}{\epsilon_d - \epsilon_r}; \quad \epsilon_t = \frac{L_0\epsilon_r - L_1\epsilon_d}{L_0 - L_1}.$$

The total strain energy released by the presence of a crack in a duplex reinforced sheet is computed by numerically integrating equations (6) and (7) over the whole elliptical zone. At each position along the crack equation (6) is used when equations (4) describe the strain distribution and equation (7) is used when equations (5) describe the strain distribution along the particular section under consideration. The rate of release of strain energy is then computed by numerical differentiation of the strain energy released at successive crack lengths. The general form of the computed rates of release of strain energy, for an unreinforced and a duplex reinforced sheet, as a function of crack length and for increasing values of applied strain is shown in figure 9.

TABLE 1. TYPICAL PROPERTIES OF A SHEET MATERIAL REINFORCED WITH NON-FRACTURING REINFORCING ELEMENTS

$E_f = 150$ GPa	$\tau = 1.5$ MPa
$E_t = 70$ GPa	$r = 0.30$ mm
$E_m = 70$ GPa	$\sigma_d = 1.10$ GPa
$E_c = 82$ GPa	$\epsilon_d = 0.00733$
$V_f = 0.15$	$G_m = 300$ KJ m^{-2}
$V_t = 0.15$	$P = 2.52 \times 10^{-2}$ m^{-1}
$V_m = 0.70$	$Q = 6.67 \times 10^{-2}$ m^{-1}

For simplicity, the elastic modulus of the tubes is assumed to be the same as that of the matrix sheet.

A list of the parameters used in the computation is given in table 1. It will be observed that for strain values up to ϵ_c, which corresponds to the stress at which the core-reinforcing elements are just capable of supporting the whole applied load, the rate of release of strain energy approaches a maximum value with increasing crack length. Up to the strain level ϵ_c the core elements nowhere decouple from the tube/sheet assembly. Therefore, the areas VRS and SQTP (figure 3) which are equal, have a maximum value and ϵ_r approaches ϵ_β with increasing crack length. To a first approximation the strain energy released is therefore proportional to the crack length and, consequently, the rate of release of strain energy approaches a limiting value with increasing crack length. This contrasts with the unreinforced sheet for which the rate of release of strain energy increases linearly with increasing crack length. Thus, provided the rate of absorption of energy exceeds this limiting value, catastrophic matrix crack growth is not energetically possible whatever the crack length. For values of strain above ϵ_c the rate of release of strain energy for the reinforced sheet is approximately proportional to the crack length but is reduced compared with the unreinforced situation.

2.6. *Theoretical equations of energy absorption*

During crack growth in a sheet reinforced with non-fracturing reinforcing elements, energy is absorbed due to the work of fracture of the tube/sheet assembly and by relative displacements between the core and tube elements against the resisting interfacial frictional forces. The rate of absorption of energy with respect to the total crack length, due to fracture of the tube/sheet assembly, is $V_m G_m + V_t G_t$ where V_m, G_m and V_t, G_t are the volume fraction and work of fracture of the sheet and tubes respectively.

The work done against frictional forces during the growth of a crack is first calculated for a reinforcing element at a distance x from the mid-point of the crack, assuming the maximum core element strain ϵ_μ is less than the debounding strain ϵ_d. During the crack growth, relative displacement between the core and tube element occurs between the crack face and the position L_1 (figure 3), so that the frictional energy losses are confined to this region.

Now the relative displacement dm_y at a distance y from the crack face is given by the integrated strain difference between the core and tube element from the position y to L_1 and is, therefore,

$$dm_y = \int_y^{L_1} \epsilon_\mu(1 - y/L_1)\, dy = \epsilon_\mu(\tfrac{1}{2}L_1 - y + y^2/2L_1),$$

where $\epsilon_\mu(1 - y/L_1)$ is the strain difference between the core and tube elements at a distance y from the crack face. ϵ_μ and L_1 are given by equations (4). Also the frictional force across a length dy of core-tube interface will be given by $2\pi r\tau\, dy$. Hence, it follows that the frictional work done by the length dy of the core element at a distance y from the crack face, during the growth of the crack is

$$2\pi r\tau\, dy\, dm_y = 2\pi r\tau\, dy\, \epsilon_\mu(\tfrac{1}{2}L_1 - y + y^2/2L_1).$$

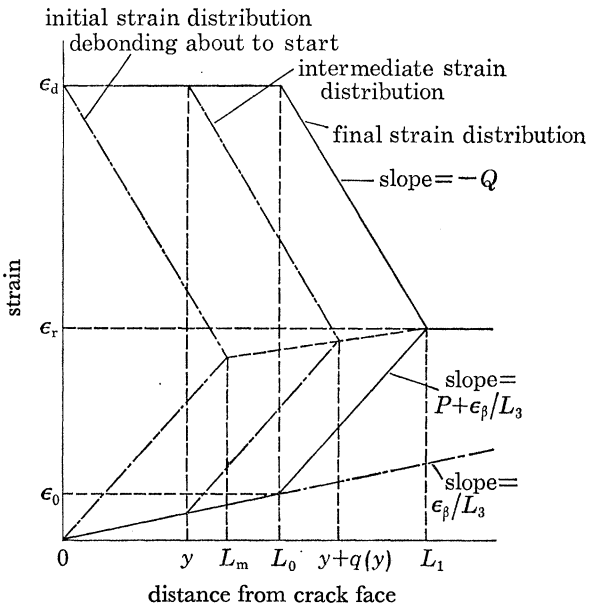

FIGURE 10. The section of the strain distribution shown in figure 4 in which the relative displacements at the core/tube interface occur.

Thus, the total work done against frictional forces by the whole core element is obtained by integrating from O to L_1 (figure 3) and is

$$2\pi r\tau \int_0^{L_1} \epsilon_\mu(\tfrac{1}{2}L_1 - y + y^2/2L_1)\, dy = \tfrac{1}{3}\pi r\tau\epsilon_\mu L_1^2.$$

The number of core elements in a section of width δx and unit thickness is $V_f\, \delta x/\pi r^2$. Thus, the work done against frictional forces in this section, for one quadrant of the partially relaxed ellipse, is given by

$$\delta W_{\Delta x} = V_f \tau\epsilon_\mu L_1^2\, \delta x/3r.$$

Substitution for ϵ_μ from equations (4) gives

$$\delta W_{\Delta x} = V_f \tau\delta x[P + Q + \epsilon_\beta/L_3]\, L_1^3/3r. \tag{8}$$

When the applied stress and crack length are such that the core elements in the section considered reach their debonding stress in the vicinity of the crack, the strain distribution is as shown in figure 4. The work done against the resisting frictional forces by a debonded core element may

be computed by considering the relative displacement between core and tube elements, at all points along the core element, up to the strain level at which the core element debonds. The region of the strain distribution in which the relative displacements occur ($0 \leqslant y \leqslant L_1$) is shown in figure 10.

First consider the intermediate situation during the development of the strain distribution with the debonded length of the core element extending to a distance y from the crack face. Stress transfer between the core and tube/sheet assembly occurs between y and $y+q(y)$ (figure 10). Thus, the relative displacement $\mathrm{d}m_y$ between core and tube element (at y) required to raise the core element strain (at y) to ϵ_d is the integrated strain difference between the core and tube elements between y and $y+q(y)$ and is given by

$$\mathrm{d}m_y = \tfrac{1}{2}(P+Q+\epsilon_\beta/L_3)\, q^2(y).$$

It is apparent from figure 10, that $q(y)$ is a linear function of y and is given by

$$q(y) = L_\mathrm{m} - (L_\mathrm{m}+L_0-L_1)\, y/L_0 \tag{9}$$

and

$$L_\mathrm{m} = \epsilon_\mathrm{d}/(P+Q+\epsilon_\beta/L_3).$$

L_1 and L_0 are given by equations (5).

Thus, the work done against frictional forces by a length of core element, $\mathrm{d}y$, in raising the strain of that length of core element at a distance y from the crack face to the debond strain level ϵ_d is

$$2\pi r\tau\, \mathrm{d}m_y = \pi r\tau(P+Q+\epsilon_\beta/L_3)\, q^2(y)\, \mathrm{d}y.$$

Relative displacement between the core and tube elements, subsequent to the core element strain reaching ϵ_d, involves no frictional work since the core element is assumed to decouple suddenly and completely from the tube. Thus, for the debonded region of the core element, which extends to a distance L_0 from the crack face, the frictional work done is obtained by integrating from O to L_0 and is

$$\pi r\tau(P+Q+\epsilon_\beta/L_3)\int_0^{L_0} q^2(y)\, \mathrm{d}y.$$

Substituting for $q(y)$ from equation (9) and integrating gives

$$\tfrac{1}{3}\pi r\tau(P+Q+\epsilon_\beta/L_3)\,[3(L_1-L_0)\, L_0 L_\mathrm{m} + L_0(L_\mathrm{m}+L_0-L_1)^2].$$

For the core element from L_0 to L_1 the frictional work done is calculated as for the non-debonded situation and is

$$\tfrac{1}{3}\pi r\tau(P+Q+\epsilon_\beta/L_3)\,(L_1-L_0)^3.$$

Thus the total work done against frictional forces by the reinforcing elements in a section of width δx and unit thickness, in one quadrant of the partially relaxed ellipse at a distance x from the centre of the crack (for $\epsilon_\mu = \epsilon_\mathrm{d}$) is

$$\delta W_{Ax} = \frac{V_\mathrm{f}\tau\delta x}{3r}(P+Q+\epsilon_\beta/L_3)\,[(L_1-L_0)^3 + 3L_0 L_\mathrm{m}(L_1-L_0) + L_0(L_\mathrm{m}+L_0-L_1)^2], \tag{10}$$

where $V_\mathrm{f}\delta x/\pi r^2$ is the number of reinforcing elements in the section.

The total strain energy absorbed frictionally can be computed by numerically integrating equations (8) and (10) over the whole partially relaxed elliptical zone around the crack. At each position along the crack, equation (8) is used when equations (4) describe the strain distribution, and equation (10) is used when equations (5) describe the strain distribution. The rate of

absorption of strain energy is then computed by numerically differentiating the strain energy absorbed at successive crack lengths.

The general form of the computed rates of absorption of strain energy, due to frictional effects, for increasing values of bulk strain are shown in figure 11. For strain levels up to ϵ_c, which corresponds to the stress at which the core elements are just capable of supporting the whole applied load (i.e. $\epsilon_\beta \leqslant \epsilon_c$), the rate of absorption of energy tends to a limiting value with increasing crack length. This occurs because the relative displacement between core and tube elements tends to a limiting value. Furthermore, comparison of figures 9 and 11 indicates that for $\epsilon_\beta \leqslant \epsilon_c$ the ratio R of the rate of absorption of strain energy (due to frictional effects) to the rate of release of strain energy rapidly approaches an upper limiting value with increasing crack length. From this and other data computed for a wide range of composite properties (I. R. McColl & J. G. Morley, unpublished work) the limiting value of this ratio in general is found to be close to a value of 0.5.

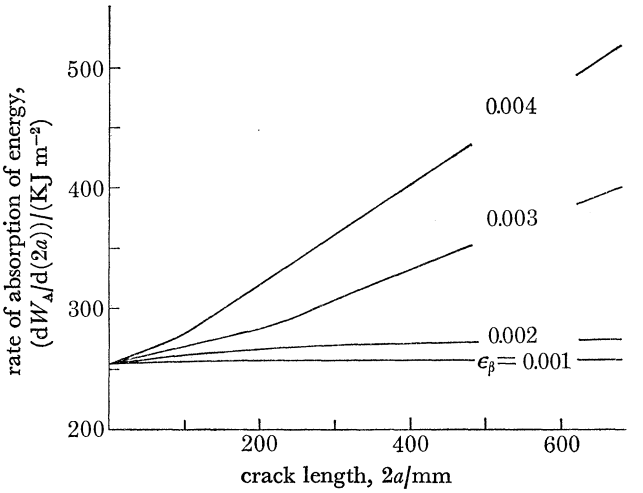

FIGURE 11. Rates of absorption of energy due to frictional effects computed using the values listed in table 1. (Rate of absorption of energy due to matrix and tubes $= V_m G_m + V_t G_t = 255$ kJ m^{-2}.)

That is, it is almost independent of the composite properties and the applied strain (provided of course $\epsilon_\beta \leqslant \epsilon_c$). For strain levels above ϵ_c debonding of the core elements occurs and the rate of absorption of energy increases with increasing crack length. Thus, the effective work of fracture increases with increasing crack length under these conditions. Comparison of figures 9 and 11 indicates that for $\epsilon_\beta > \epsilon_c$ the ratio R again approaches an upper limiting value with increasing crack length. However, in contrast to the situation for $\epsilon_\beta \leqslant \epsilon_c$ the upper limiting value of the ratio R is strongly dependent on the composite properties and decreases as the applied strain ϵ_β is increased. Data computed for a wide range of composite properties indicates that the maximum limiting value of the ratio R, which occurs for a value of applied strain ϵ_β slightly above the critical strain ϵ_c, may exceed 0.5 (maximum value of R for $\epsilon_\beta \leqslant \epsilon_c$) and indeed may approach unity. Hence, for all values of applied strain the frictional energy loss term is of major importance since it may considerably reduce the matrix work of fracture necessary to ensure crack stability.

It should be noted that the strain energy absorbed by a particular section at a particular crack length is calculated (for simplicity) assuming the matrix strain gradient (ϵ_β/L_3) is fixed during the development of the strain distribution along the section. Under real conditions the crack would extend in stages to the final length and the value of L_3, for the particular section considered, would

increase correspondingly up to the final value. For the case of non-debonded core elements, the value of L_3 during the development of the strain distribution along a section does not affect the total relative displacement between the core and tube elements and, hence, the energy absorbed frictionally. However, during the development of the strain distribution along a section in which the core elements are debonded, the relative displacement between the core and tube elements (for the intermediate situation shown in figure 10) depends on the value of ϵ_0 and thus the matrix strain gradient ϵ_β/L_3. The value of the frictional work done increases to some extent with increasing L_3. Thus, the method used to compute the frictional work done, for debonded core elements, overestimates this term to some extent.

3. Validity of the theoretical model of strain distribution

The model used is based on three simplifying assumptions.

(*a*) The strain field around the crack in the matrix sheet is assumed to be linear.

(*b*) The strain distribution of the crack bridging core elements is assumed linear up to a critical strain level at which complete decoupling is assumed to occur.

(*c*) The elliptical zone around the crack is assumed to be divided up, in effect, into a number of parallel segments perpendicular to the crack so that each segment is subjected only to longitudinal loads applied in a direction perpendicular to the length of the crack.

Assumption (*a*) is a reasonable approximation to the actual strain distribution around a crack in a unidirectionally loaded elastic sheet (Inglis 1913). As stated above, the size of the elliptical zone and, hence, the strain gradients are chosen so that the amount of strain energy released by the presence of the crack is equal to that obtained in the classical case. In the case of a real duplex fibre core decoupling occurs progressively, not instantaneously as assumed in the theory set out above. The strain distribution chosen, however, corresponds quite closely to those of experimental systems and the major uncertainty seems likely to be associated with the contribution to the effective work of fracture by the frictional energy loss term when debonding of the core elements is assumed to occur instantaneously. The assumption that the composite structure, within the elliptical zone around the crack, carries only loads aligned in a direction perpendicular to the crack seems to be a reasonable approximation. It is clear from an inspection of the strain field around the crack that, over the major portion of the elliptical zone, the strain distributions for adjacent segments are similar. Thus, the strain energy generated by shear displacements would not appear likely to be of major importance in a more comprehensive assessment of the strain energy release rate.

4. Theoretical predictions of the analysis

The analysis indicates that, provided the core members are capable of carrying the whole of the tensile load applied to the composite structure, the rate of release of strain energy by a transverse crack in the matrix will tend to some upper limiting value as the length of the crack increases. Clearly, if this value is less than the matrix work of fracture, catastrophic matrix crack growth will not be possible whatever the crack length. The analysis also predicts that the effective work of fracture will be enhanced by the frictional energy losses encountered during crack growth. The importance of this factor, relative to the work of fracture of the tube sheet assembly, increases with increasing crack length particularly when debonding occurs. As a consequence it would

PHILOSOPHICAL TRANSACTIONS OF THE ROYAL SOCIETY A MATHEMATICAL, PHYSICAL & ENGINEERING SCIENCES

seem that very long matrix cracks can remain stable even when the non-fracturing reinforcing elements are not capable of carrying the whole of the applied load.

In order to provide some experimental data on matrix crack growth in systems of this type, reinforced sheet structures have been constructed using two types of matrix material. The reinforcing elements have been similar in each case but the work of fracture and elastic characteristics of the two sheet materials used have been very different. This work is described in the following section.

5. Experimental observations

5.1. *Experimental samples*

Experimental specimens were fabricated from two types of sheet (matrix) material, with widely different work of fracture and elastic characteristics. These materials were half-hard brass shim strip (0.055 mm thick) and polymethylmethacrylate (ICI Perspex) sheet (1.50 mm thick). Specimens fabricated from the former used either a single strip (152 mm wide) or a number of parallel strips soldered together, with 6 mm wide lap joints, to produce a large sheet (approximately 1 m square). This rather unsatisfactory fabrication technique caused buckling to occur in the metal sheets but was necessary, owing to the non-availability of suitably thin material of sufficient width. The use of such thin material was essential because of the limited capacity of the available test equipment.

The reinforcing elements used were formed from either 10 mwg stainless steel wire or 11 mwg tinplated piano wire together with 19 gauge stainless steel hypodermic tubing. The helical core elements were produced by first close-winding the wire on to a mandrel and then extending the resulting close-wound spring, by plastically deforming the wire, into the form of a large angled helix (helix angle approximately 85°).

The theoretical model outlined in § 2 assumes that the core elements are initially under zero longitudinal tensile stress. In order to satisfy this condition experimentally the tube elements were cut into short lengths. This was necessary because if a helical core element is pulled into a tube and the external load is then removed the core element remains in tension and the tube in corresponding compression. Since the residual core tensile load is proportional to the length of the core/tube interface, the use of short tube elements (20 mm) results in a residual core tensile load sufficiently small to be neglected. The reinforcing elements were assembled by threading the short tube elements on to the core wire which was held in tension slightly above the debonding stress. A small gap of 1.0 mm was left between each short tube element. The core element tensile load was removed and the bicomponent reinforcing element was attached to the sheet at the midpoint of each short tube element. The short tube elements were directly soldered to the brass sheet. In the case of the Perspex sheets, the short tube elements were soldered to an array of washers which were attached to the sheet by screws. Because of their discontinuous form the tube elements did not directly interfere with crack propagation in either type of matrix sheet.

As discussed elsewhere (Morley *et al.* 1976), the effective Young modulus of the core element when constrained within the tube can be appreciably greater than that of the helix when loaded separately. This enhanced core element stiffness, together with the effective contribution of the tubes and their attachments to the stiffness of the sheets, were determined from modulus measurements on sections of the reinforced specimens. An example is given in table 2 of the elastic properties of a typical reinforcing element.

A single, uniformly spaced, parallel array of duplex elements was attached to one side of the

brass sheets and similar arrays were attached to both sides of the reinforced Perspex specimen. The reinforcing elements were attached in a direction perpendicular to that of the initial crack. In the case of the reinforced specimens this was in the sheet material only – the core elements remained bridging the initial crack.

TABLE 2. PROPERTIES OF A TYPICAL NON-FRACTURING REINFORCING ELEMENT

core element material	12 m.w.g. tinplated piano wire
core element diameter	0.73 mm
tube material	19 gauge stainless steel hypodermic tubing
tube internal diameter	0.795 mm
tube external diameter	1.065 mm
mandrel diameter	1.23 mm
core element prestress	1660 MPa
core element debonding stress	1100 MPa
core element free amplitude	0.82 mm
straight wire Young modulus	195.4 GPa
free helix Young modulus	152.2 GPa
constrained helix Young modulus	185.5 GPa

TABLE 3. REINFORCING ELEMENTS

	type (*a*)	type (*b*)
core element material	10 m.w.g. stainless steel wire	11 m.w.g. tinplated piano wire
core wire diameter/mm	0.61	0.66
mandrel diameter/mm	1.04	1.06
preload/N	350	480
core element wavelength/mm	5.9	6.3
core element free amplitude/mm	0.86	0.88
tube element material	19 gauge stainless steel hypodermic tubing	19 gauge stainless steel hypodermic tubing
tube inside diameter/mm	0.80	0.83
tube outside diameter/mm	1.06	1.08
pull in stress/MPa ~ limiting debonding stress	1280	1350†
mean core/tube shear strength/MPa	1.3	1.0
constrained core element Young modulus/GPa	91.0	119.6
free core element Young modulus/GPa	63.0	97.9
core wire modulus in original straight condition/GPa	146.0	192.3
tube element Young modulus/GPa	167.0	171.1

† Variations were observed in the characteristics of nominally similar material. The material used was selected so as to be as nearly uniform as practicable.

In the case of the brass sheet specimens the initial crack was cut with a scalpel blade. The initial crack in the Perspex sheets was a saw cut (1.2 mm wide). Crack tips were formed at the ends of the saw cut using a steel wedge and an impact below.

Details of the experimental specimens are listed in tables 3–5.

5.2. *Experimental arrangements*

The sheet specimens were tested under fixed grip conditions in an Instron universal testing machine. The specimens were held between parallel rigid beams clamped across their ends. Both beams were attached to the testing machine by pivoted couplings. The loads were applied perpendicular to the initial crack, i.e. parallel to the reinforcing elements and perpendicular to

PHILOSOPHICAL TRANSACTIONS OF THE ROYAL SOCIETY A MATHEMATICAL, PHYSICAL & ENGINEERING SCIENCES

the soldered lap joints when present. All the tests were performed at an extension rate of 0.2 mm min^{-1}.

5.3. *Experimental results*

Figure 12 shows the experimentally observed stress-indicated strain diagrams obtained for the specimens detailed in tables 4 and 5. The stress is taken as the average stress over the whole specimen and the indicated strain is the observed extension divided by the nominal gauge length.

TABLE 4. UNREINFORCED SHEET SPECIMENS

	specimen number			
material	1*a* brass	2*a* brass	3*a* brass (fabricated)	4*a* Perspex
thickness/mm	0.055	0.055	0.055	1.41
gauge length/mm	465	470	910	900
width/mm	120	152	915	298
initial crack length/mm	41.0	41.0	200.0	72.0
Young modulus/GPa	97.9	97.9	97.9	2.88
work of fracture, obtained from critical stress, Gm_1/(kJ m^{-2})	6.0	6.0	11.8	0.45
direction of crack†	⊥	⊥	∥	—
work of fracture, obtained for double cantilever beam technique. Average value over whole fracture process, Gm_2/(kJ m^{-2})	33.0	33.0	50.0	0.40
work of fracture, obtained for double cantilever beam technique. Value computed from compliance at initiation of fracture, Gm_3/(kJ m^{-2})	—	—	14.2	—

† Perpendicular or parallel to rolled direction.

TABLE 5. REINFORCED SHEET SPECIMENS

	specimen number				
sheet material	1*b* brass	2*b* brass	3*b* brass	3*c* brass	4*b* Perspex
reinforcing element type	(*b*)	(*b*)	(*a*)	(*a*)	(*b*)
sheet thickness/mm	0.055	0.055	0.055	0.055	1.57
gauge length/mm	465	470	872	865	895
sheet width/mm	120	152	915	860	299
initial crack length/mm	40.5	41.0	200.0	200.0	72.0
core element volume fraction	0.224	0.233	0.054	0.101	0.043
effective tube element volume fraction	0.051	0.052	0.014	0.027	0.013
sheet material volume fraction	0.725	0.715	0.932	0.871	0.944
work of fracture of sheet material, obtained from corresponding unreinforced specimen/(kJ m^{-2})	33.0	33.0	50.0	50.0	0.40

The behaviour of the unreinforced sheets was approximately as predicted by the Griffith–Irwin theory, catastrophic failure occurring at a critical stress value. The work of fracture values Gm_1 calculated from the critical stress values, using the Griffith–Irwin theory, were compared with values obtained for similar material under conditions of double cantilever beam crack propagation. These work of fracture values were calculated by two methods. Firstly, the work of fracture Gm_2 was simply obtained from the work done to fracture a specimen completely in a controlled manner. Secondly, in the case of crack propagation in the brass shim parallel to the

rolled direction, the work of fracture Gm_3 was calculated using a slightly modified compliance analysis method described by Shockley & Groves (1968). Gm_2 is an average value for the whole fracture process and Gm_3 is the effective work of fracture value pertaining to the initiation of fracture.

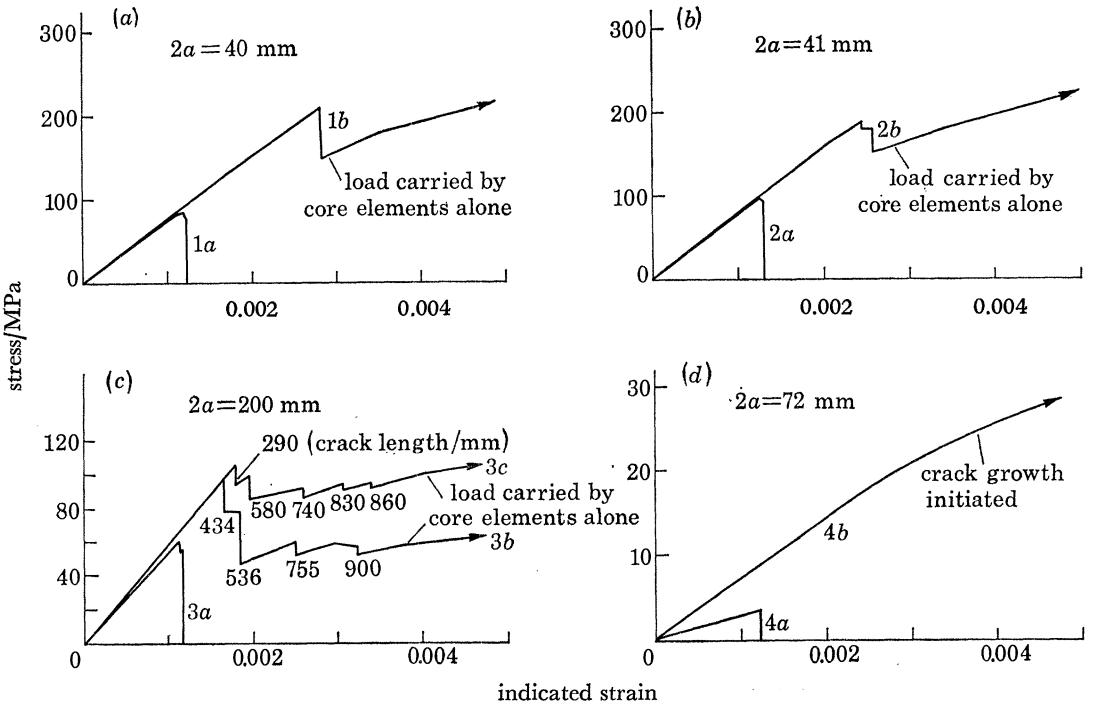

FIGURE 12. Observed stress-indicated strain diagrams for unreinforced sheets and the corresponding sheets reinforced with non-fracturing reinforcing elements. Specimens: (*a*) 1*a*, 1*b*; (*b*) 2*a*, 2*b*; (*c*) 3*a*, 3*b*, 3*c*; (*d*) 4*a*, 4*b*.

Inspection of table 4 shows that in the case of the brass sheets both Gm_2 and Gm_3 exceed Gm_1. In particular Gm_2 is considerably larger than Gm_1. Some appreciable difference between Gm_1 and Gm_2 might have been anticipated since similar values would only be expected when the fracture initiation and fracture propagation processes are similar. It was obvious from an inspection of the crack profiles that, in the case of the stable crack growth experiments, the crack profile deviated appreciably from that of a plane cleavage crack. Thus, since the crack lengths from which values of Gm_2 were calculated did not take account of these deviations, the resultant value of Gm_2 would be expected to be appreciably larger than the work done per unit area of fractured material.

Since Gm_1 and Gm_3 both pertain to the initiation of fracture from similar initial cracks, their values would be expected to be similar. The observed difference in values may be due to two factors, which may also contribute to the difference between Gm_1 and Gm_2. Firstly, neither the individual brass sheets (which formed the smaller specimens) nor the larger specimens (which were fabricated from a number of narrow sheets) were completely flat. As the applied load was increased it was apparent that, for both types of specimens, the central regions in which the crack was situated were carrying a higher than average stress. Also the larger sheets, in particular, were slightly buckled on a scale of the order of 10 mm so that, in the case of these specimens, small-scale perturbations in the stress field were superimposed on the larger-scale non-uniformity previously mentioned. The general non-uniformity in the stress field would be expected to initiate crack

growth at a lower nominal stress than would have been expected for a perfectly flat sheet subjected to a uniform tensile stress. The second (micro) effect would be expected either to enhance or to reduce the nominal stress at which crack initiation occurred, depending on the position of the crack tip with respect to the small-scale stress perturbations. The second factor requiring consideration is the appreciable value of the crack length to sheet width ratio (see table 4). This would be expected to enhance the stress concentration effect of the crack. In the case of the reinforced sheets the situation is further complicated by the presence of the crack bridging load bearing reinforcing members.

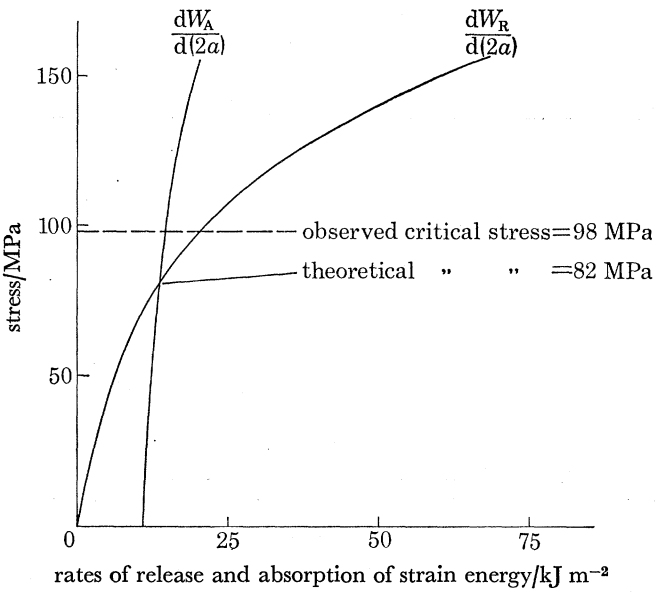

FIGURE 13. Rate of release, $dW_R/d(2a)$, and rate of absorption, $dW_A/d(2a)$, of strain energy, as a function of the applied stress, computed from the data for specimen no. 3*b*. Initial crack length, $2a = 200$ mm.

In the case of the Perspex specimens Gm_1 was observed slightly to exceed Gm_2. Although the problems of non-uniform loading and localized buckling were not encountered with the Perspex specimens, the value of the crack length to sheet width ratio was similar to that of the brass specimens. Thus, assuming the fracture initiation and propagation processes to be similar, the value of Gm_2 would be expected to be larger than the observed value of Gm_1. However, observations by Davidge & Tappin (1968) indicate that the fracture processes are different and that in fact Gm_1 should exceed Gm_2 (by a factor of approximately 2). Thus the error in the observed value of Gm_1 and the difference in the true value of Gm_1 and Gm_2, due to the different fracture processes, might be expected to cancel and result in the observed similarity of Gm_1 and Gm_2.

A very important observation was that crack propagation in the reinforced specimens commenced at a substantially higher critical stress and corresponding strain value than was observed for their unreinforced counterparts. This is a clear indication of the ability of the crack bridging reinforcing elements to inhibit the growth of a crack in the matrix sheet. It is felt that the observed differences in nominal stress values for crack growth in the reinforced and unreinforced metal sheets provides a valid basis of comparison despite the uncertainties about the magnitude of local stress perturbations discussed above. The matrix of the narrow reinforced brass specimens (nos. 1*b* and 2*b*) failed by fast crack propagation from the initial crack (figures 12*a* and 12*b*). However,

the large reinforced brass specimens (nos. 3*b* and 3*c*) did not fail by fast crack propagation through the matrix sheet (figure 12*c*). Instead, the matrix crack propagated in a stable manner as the applied strain was increased. In the case of the reinforced Perspex sheet (figure 12*d*) the initial crack did not completely propagate to the edge of the sheet. A limited amount of stable crack growth occurred as the applied strain was increased until eventually progressive failure of the matrix occurred at the ends of the specimen, where stress transfer from the sheet to the reinforcing elements occurs. In this region the core elements do not contribute fully to the strength of the structure.

In all the reinforced sheets the core elements remained bridging the crack and continued to support an appreciable applied load, even when the crack extended across the whole width of the sheet. Thus they provided a residual fail-safe tensile load bearing capability.

5.4. *Comparison of experimental data with theory*

The theory outlined in § 2 was used to compute rates of release and absorption of strain energy from the experimental specimen data listed in tables 4 and 5. Figure 13 shows the rates of release and absorption of energy computed for the large reinforced brass sheet specimen, number 3*b*. The rates of release and absorption of strain energy are plotted as a function of the applied stress for a value of crack length corresponding to the experimental initial crack length. The point of intersection of the curves gives the predicted critical stress value for a reinforced sheet containing a crack of the length considered. Also indicated in figure 13 is the corresponding experimentally observed critical stress value.

TABLE 6. OBSERVED AND COMPUTED CRITICAL STRESS VALUES

specimen number	initial crack length 2*a*/mm	observed critical stress/MPa	computed critical stress/MPa
1*b*	40.5	209.0	148.0
2*b*	41.0	187.0	133.0
3*b*	200.0	98.0	82.0
3*c*	200.0	106.5	88.0
4*b*	72.0	27.0	21.0

Table 6 lists the experimentally observed and the corresponding computed critical stress values for the reinforced specimens detailed in table 5. It will be observed that the computed critical stress values are in reasonable agreement with the experimentally observed values but that, in all cases, the experimental value exceeds the computed value.

The work of fracture values, used to compute the predicted critical stress values for the reinforced sheets, were obtained by applying the unmodified Griffith equation to the critical stress values obtained for the corresponding unreinforced sheets. The various factors considered in the choice of the most appropriate work of fracture value have been outlined in § 5.3. It is felt to be reasonable to use these particular work of fracture values since they are the values obtained at the onset of crack growth. Also they are for sheets of similar size and having similar initial crack lengths to the corresponding reinforced specimens. Thus, stress concentrations owing to the finite width of the sheets and to non-uniform loading of the sheets (because of buckling, etc.), would be expected to be similar for both the unreinforced and the similar reinforced sheets. Also variations in the work of fracture as a function of crack length, as a result of the development of the plastic zones, should be overcome by comparing unreinforced and reinforced sheets with similar initial crack lengths. The work of fracture value may be underestimated by assuming the

stress distribution of the unreinforced sheet to be that of a semi-infinite sheet. However, the error caused by using the semi-infinite sheet stress distribution to compute the predicted critical stress value for the reinforced sheet should be largely overcome by using this underestimated work of fracture value obtained for an unreinforced sheet of similar size and with a similar initial crack length.

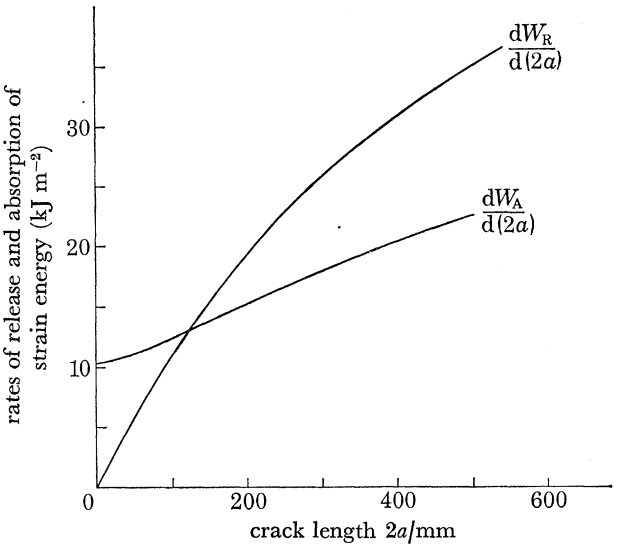

FIGURE 14. Rates of release and absorption of strain energy, as a function of crack length, computed from the data for specimen no. 3c. Applied stress = 99 MPa.

The theoretical model outlined in § 2 predicts that, at a particular value of critical stress, a matrix crack in a reinforced sheet should become energetically unstable. However, the matrix crack propagation observed in specimens 3b, 3c and 4b proceeded in a semi-stable manner (figures 12c and 12d). A possible explanation for this behaviour may be obtained from an inspection of figure 14. This is a plot of the rates of release and absorption of strain energy as a function of crack length. The values, which are computed from the data listed in table 5, are appropriate to the large reinforced brass sheet specimen number 3c. It shows that, at crack lengths sufficiently long to be predicted as energetically unstable, the difference between the rates of release and absorption of energy is relatively small. Hence, small perturbations in the stress field, such as would be produced by the micro-buckling previously mentioned, could modify the release of strain energy sufficiently to arrest the crack. Thus, an increasing applied strain would be necessary to sustain crack growth.

Also in the case of the large brass sheets, as the crack extended towards the edges of the sheet, the crack tips propagated into regions of diminishing stress. Hence, again it might be expected that an increasing applied strain would be necessary to sustain crack growth.

6. CONCLUSIONS

The basic theory outlined in § 2, dealing with the energetics of crack growth in reinforced systems utilizing non-fracturing reinforcing members, contains many simplifications. However, the observed properties of the experimental specimens so far studied are in tolerable agreement with the predictions of the theory despite the experimental difficulties encountered in their fabrication. The fail-safe capability of the reinforced sheets under tensile loading and the very

considerable modifications made to the crack growth characteristics by the reinforcing members have been demonstrated unambiguously.

It should be noted that, in these composite systems, the reinforcing members are fully load bearing (up to their debonding strain) and are not behaving parasitically, in the sense of increasing the weight of the structure for a given tensile load bearing capability. Also the metal duplex elements produce no significant impairmant of the specific stiffness of the composite structure in comparison with an unreinforced sheet. Although the core reinforcing members are convoluted their effective longitudinal elastic modulus values can be arranged to be very similar to those of the corresponding straight reinforcing member (table 2).

The analysis developed in § 2 indicates that the capability of the primary reinforcing elements to influence matrix crack growth is due to two mechanisms. Firstly, the ability of the core elements to bridge and transfer load across a matrix crack (irrespective of length or crack face separation) can reduce dramatically the release of strain energy owing to the presence of the crack. Secondly, during matrix crack extension, differential displacements between the core and sheath elements against the resisting interfacial frictional force, result in the irreversible absorption of strain energy. The former mechanism is of particular importance when the core elements are capable of carrying the total applied load. Under these circumstances, provided the sum of the matrix work of fracture and the frictional energy loss term is sufficient, a completely crack insensitive material is achievable. The frictional term is generally of particular importance when the applied strain and crack length are such that the rate of release of strain energy exceeds the work of fracture of the matrix sheet and, in these circumstances, can ensure crack stability.

The experimental reinforced sheet specimens described in this paper utilize a discontinuous sheath element to enable the core elements to be nominally under zero initial longitudinal stress. It appears possible to achieve this initial stress condition using techniques appropriate to continuous manufacturing processes. One such technique consists of first sliding a core element into a tube with an internal diameter greater than the free outside diameter of the core element. By use of conventional tube drawing techniques the internal diameter of the tube can be reduced to a suitable value less than the free external diameter of the core element. A frictional interface is thus developed with the core element under zero longitudinal stress. Preliminary observations of the behaviour of a system of this type have been reported elsewhere (Millman & Morley 1976). A second technique dispenses with the use of a hypodermic tube as the sheath element. Instead the core elements are sandwiched between two thin corrugated metal sheets. The size of the corrugations is such that, when the sheets are correctly aligned and seam welded together, a parallel array of tubes of the appropriate internal diameter is formed. Preliminary studies carried out by R. S. Millman (unpublished work) have demonstrated the general feasibility of this approach. This technique is of particular interest since the longitudinal tensile stress of the core elements can be set to any value before the sheets are welded together. This provides a convenient method for prestressing the sheet structure in compression. As discussed in § 1, prestressing of the matrix is likely to be of particular importance when fatigue loading is considered.

The overall dimensions of the experimental specimens used, and those of the initial crack lengths, correspond with typical highly stressed engineering structures where failure by catastrophic crack growth must be avoided. The strain values used also cover those of typical engineering design strains. The calculations illustrated in figures 9 and 11 correspond to a hypothetical reinforced structure consisting of an aluminium alloy sheet reinforced with non-fracturing reinforcing members having characteristics similar to those of the laboratory specimens

so far produced. It is of interest to note that, at conventional engineering design strains (0.1–0.2 %), the work of fracture of the aluminium sheet is considerably greater than the predicted value necessary to prevent unstable crack growth. For composite systems of this type, therefore, it becomes feasible to consider modifications to the alloy composition which would reduce its work of fracture and retain the crack stability feature, but enhance other desirable characteristics. Additionally, or alternatively, a further component could be added to the composite structure which could have a lower work of fracture but possess other desirable properties. One obvious candidate material for this purpose would be resin bonded carbon fibres which could be bonded directly to the metal plate. By this means the longitudinal specific stiffness of the composite structure could be increased and unstable crack growth still prevented. It seems reasonable to suppose that such a structure could accept local damage, which might cause plastic deformation of the metal sheet and fracture of the ceramic stiffening fibres, while still maintaining the fail-safe and damage tolerant characteristics conferred by the presence of the non-fracturing reinforcing members.

In figures 5 and 6 the approximate strain distributions which would be expected to occur around a crack in an aluminium sheet reinforced with steel wire/hypodermic tube duplex elements are shown. Engineering design strains would not exceed 0.2 % for most situations and the diagrams indicate that for these circumstances the core element stress transfer lengths would be of the order of 100 mm. This would be the situation whether the load was transferred from the sheet metal 'matrix' to the core members (corresponding to a conventional fibrous composite) or whether a concentrated tensile load was applied to the composite system via the core members. For the latter situation the analysis given in § 2 is applicable if one half of the stress-field is considered and the crack in the sheet metal matrix is assumed to be infinitely long. If the former loading condition is assumed the analysis given in § 2 would be applicable to crack stability in the matrix sheet in regions which are an appreciably greater distance than 100 mm from the free end of the structure. It thus applies to engineering structures of appreciable dimensions.

It will be noted that, when a concentrated tensile load is carried by the core members as a consequence of centrifugal loads carried by the composite system, the overall dimensions of the component need not exceed about 100 mm, for the system considered, and could indeed be less. The analysis of crack stability given above would not, of course, be directly applicable to this situation since the matrix would be subjected to a compressive load generated by the centrifugal forces.

The work described above has been concerned with composite structures comprising sheet metal which has been reinforced by non-fracturing reinforcing members. However, the theoretical analysis set out in § 2 is broadly applicable to matrix cracking in more conventional composites. In glass fibre reinforced polymers, for example, stress transfer between fibres and matrix takes place primarily as a result of frictional effects. Therefore, provided that the failing strain of the fibres is not exceeded and the matrix has the lower failing strain and, also, that any energy losses due to chemical debonding effects are ignored, the theory should describe the energetics of transverse matrix cracking in simple unidirectional fibrous composites (McColl & Morley 1977*b*).

This work has been carried out with the support of the Science Research Council. We thank Mr J. M. J. Bennett for fabricating the experimental specimens and invaluable assistance in their testing.

PHILOSOPHICAL TRANSACTIONS OF THE ROYAL SOCIETY A MATHEMATICAL, PHYSICAL & ENGINEERING SCIENCES

References

Chappel, M. J., Morley, J. G. & Martin, A. 1975 *J. Phys.* (D: appl. Phys.) **8**, 1071.

Davidge, R. W. & Tappin, G. 1968 *J. Mater. Sci.* **3**, 165.

Griffith, A. A. 1920 *Phil. Trans. R. Soc. Lond.* A **221**, 163.

Hancock, J. R. 1974 In *Composite materials*. Vol. 5, *Fracture and fatigue* (ed. L. J. Broutman), chap. 9, p. 371. New York: Academic Press.

Inglis, G. E. 1913 *Trans. Inst. Naval Architects*, LV, Part 1, 219.

Mayer, N. J. 1974 *Composite materials* (eds. L. J. Broutman & R. H. Krock), vol. 3, chap. 2. New York and London: Academic Press.

McColl, I. R. & Morley, J. G. 1975 *J. Phys.* (D: appl. Phys.) **8**, L100.

McColl, I. R. & Morley, J. G. 1977*a* *J. Phys.* (D: appl. Phys.) **10**, 599.

McColl, I. R. & Morley, J. G. 1977*b* *J. Mater. Sci.* **12**, 1165.

Millman, R. S. & Morley, J. G. 1976 *Mater. Sci. Enging* **23**, 1.

Morley, J. G. 1970 *Proc. R. Soc. Lond.* A **319**, 117.

Morley, J. G. 1976 *Int. Metals Rev.*, Review 208, p. 153.

Morley, J. G. & Chappell, M. J. 1977 *Composites*. **8**, 33.

Morley, J. G. & Millman, R. S. 1974 *J. Mater. Sci.* **9**, 1171.

Morley, J. G. & McColl, I. R. 1975 *J. Phys.* (D: appl. Phys.) **8**, 15.

Morley, J. G., Millman, R. S. & Martin, A. 1976 *J. Phys.* (D: appl. Phys.) **9**, 1031.

Prewo, K. M. 1976 *Proceedings of the* 1975 *International Conference on Composite Materials* (eds. E. Scala, E. Anderson, I. Toth & B. R. Noton), vol. 2, p. 817. The Metallurgical Society of AIME, 345, East 47th Street, New York.

Shockley, P. A. & Groves, G. W. 1968 *J. Am. ceram. Soc.* **51**, 299.

Zender, G. E. & Dexter, H. B. 1968 *NASA TN* 4878.

PHILOSOPHICAL TRANSACTIONS OF THE ROYAL SOCIETY A MATHEMATICAL, PHYSICAL & ENGINEERING SCIENCES